

<https://doi.org/10.1038/s41612-024-00599-0>

Enhanced North Pacific Victoria mode in a warming climate

Check for updates

Kai Ji^{1,2}, Jin-Yi Yu³, Jianping Li⁴, Zeng-Zhen Hu⁵, Yu-Heng Tseng⁶, Jian Shi⁷, Yingying Zhao⁸, Cheng Sun⁹ & Ruiqiang Ding^{1,10} ✉

The Pacific Decadal Oscillation (PDO), renowned as the dominant sea surface temperature (SST) fluctuation in the North Pacific and extensively scrutinized for its extensive influence on global climate patterns, stands in stark contrast to the Victoria mode (VM). Traditionally, the VM, representing the second most prominent SST pattern in the North Pacific, has not garnered comparable attention. However, our investigation unveils a remarkable surge in the low-frequency VM variability, spanning periods greater than 8 years, over the course of a century. Astonishingly, this enhanced VM variability now surpasses the PDO's variability in recent decades, signifying a notable shift. Consequently, the heightened VM variability assumes newfound significance in shaping climate systems across the entire North Pacific region and in distant locales. This intensified VM behavior could be attributed to amplified atmospheric variability in the Hawaiian region, primarily stemming from the reinforced variability in the tropical central Pacific (CP) SST in recent decades. As greenhouse warming escalates CP SST variability, the VM's enhanced variability may further intensify, yielding broader and more profound repercussions in the future.

The North Pacific, extending from the tropics to the Arctic region, plays a crucial role in influencing weather and climate across both nearby and distance areas due to its sea surface temperature (SST) variability^{1–3}. The Pacific Decadal Oscillation (PDO), characterized as the primary empirical orthogonal function (EOF) of SST anomalies in the extratropical North Pacific (Supplementary Fig. 1a), represents the most notable SST variability in the North Pacific. It exhibits long-term fluctuations on an inter-decadal timescale^{4–6}, exemplified by the renowned 1976/1977 regime shift^{7,8}, a subject of extensive research due to its far-reaching effects on global climate, natural resources, and marine and terrestrial ecosystems^{4,5,9–14}.

The second prominent mode of variability in North Pacific SST, known as the Victoria mode (VM, defined as the second EOF of SST in the extratropical North Pacific)¹⁵, or alternatively referred to as the North Pacific Gyre Oscillation (NPGO, defined as the second EOF of sea surface height (SSH) in the central and eastern North Pacific)¹⁶, exhibits a distinctive

northeast-to-southwest SST dipole pattern across the extratropical North Pacific (Supplementary Fig. 1b, c). While the VM/NPGO has not been considered a primary source of variability, it has garnered increasing attention in climate studies over the past two decades due to its far-reaching implications for various climate systems spanning the pan-North Pacific region. These implications encompass phenomena such as El Niño–Southern Oscillation (ENSO)^{17–22}, the Pacific Intertropical Convergence Zone (ITCZ)²³, marine heatwaves (MHW) in the northeast Pacific^{2,24,25}, tropical cyclones (TC) in the western North Pacific²⁶, particulate pollution in North China²⁷, rainfall patterns in South China²⁸, surface air temperature (SAT) in eastern North America^{29,30} and Eurasia²⁹, as well as sea surface salinity (SSS) and nutrient distribution in the eastern North Pacific³¹. Given the widespread and profound climatic impacts associated with the VM/NPGO, there is a pressing need to comprehensively understand the recent and possible future changes in its variability and the resulting consequences for climate systems.

¹State Key Laboratory of Earth Surface Processes and Resource Ecology, Beijing Normal University, Beijing, China. ²Department of Atmospheric Science, School of Environmental Studies, China University of Geosciences, Wuhan 430074, China. ³Department of Earth System Science, University of California, Irvine, CA 92697, USA. ⁴Frontiers Science Center for Deep Ocean Multispheres and Earth System (FDOMES)/Key Laboratory of Physical Oceanography/Institute for Advanced Ocean Studies, Ocean University of China, Qingdao, China. ⁵Climate Prediction Center, NCEP/NWS/NOAA, 5830 University Research Court, College Park, MD 20740, USA. ⁶Institute of Oceanography, National Taiwan University, Taipei, Taiwan. ⁷Physical Oceanography Laboratory/Frontier Science Center for Deep Ocean Multispheres and Earth System/Sanya Oceanographic Institution, Ocean University of China, Qingdao, China. ⁸Laoshan Laboratory, Qingdao, China. ⁹State Key Laboratory of Remote Sensing Science, College of Global Change and Earth System Science, Beijing Normal University, Beijing, China. ¹⁰Key Laboratory of Environmental Change and Natural Disasters of Chinese Ministry of Education, Beijing Normal University, Beijing, China. ✉e-mail: drq@bnu.edu.cn

Nevertheless, a comprehensive exploration of the alterations in VM/NPGO variability and their associated climatic effects within a prolonged warming climate remains incomplete. In this context, utilizing a diverse array of data sources, we present compelling evidence for a substantial rise in low-frequency VM/NPGO variability spanning a century from 1920 to 2021. We emphasize the significant contribution of the intensified variability in tropical central Pacific (CP) SST variability to the augmented VM/NPGO variability. These results imply that the heightened VM/NPGO pattern may assumed an increasingly pivotal role in shaping pan-North Pacific climate variability.

Results

Increased VM variability

We first calculated the 23-year running root-mean-square (RMS) of the VM index during the winter–spring seasons (December–May) for the period 1920–2021 (see Data and Methods). These seasons were selected because they are when the VM typically develops and peaks^{15,17}. Over a century-long timespan, the VM variability exhibits a significant increasing trend (Fig. 1a; see Data and Methods). In particular, the low-frequency variability (>8 years) of the VM primarily contributes to the overall increased VM variability (Supplementary Figs. 2 and 3a–c). Similarly, the variability of the VM’s SSH counterpart, the NPGO¹⁶, also displays a distinct increasing trend based on available SSH data for the period 1950–2021 (Supplementary Fig. 4a; see Data and Methods). Given the close tracking relationship between the VM and NPGO^{16,32}, especially at low-frequency timescales (>8 years; see also Supplementary Fig. 4b), our subsequent focus shifted to examining changes in VM variability unless stated otherwise.

In contrast to the increased variability observed in the VM, the typical low-frequency fluctuations of the PDO with a 5–30-year periodicity have narrowed down to 10–15 years around the 1980s to 1990s, and decadal variations within the 15–30-year band are nearly absent (Supplementary Fig. 3d–f). Consequently, the low-frequency variability (>8 years) of the PDO exhibits a significant decreasing trend (Fig. 1a). Furthermore, we examined the secular variations in the ratio of the low-frequency variability (>8 years) between the VM and PDO indices.

Of particular interest is the observation that this ratio has consistently exceeded 1.0 after the early 1990s (Fig. 1b). This suggests that in recent decades, the intensity of the VM has surpassed that of the PDO. As expected, we have also noted an increase in the frequency of VM events (defined as |VM index| greater than 0.5 standard deviation) and a decrease in PDO events (defined as |PDO index| greater than 0.5 standard deviation) in recent decades (Fig. 1c). In tandem with the heightened VM variability, there is a noticeable increase in VM-like SST anomalies in the North Pacific, consistent with increasing in the explained variance of the VM (EOF2; see Supplementary Fig. 5). This is demonstrated by a strong and statistically significant positive correlation between VM-related SST anomalies and observed SST anomalies in recent decades (see Fig. 1d).

The significant rise in VM variability and the corresponding decrease in PDO variability have been consistently observed across various SST datasets and over different time spans using varying moving window lengths (Supplementary Fig. 6). These findings underscore the robustness of the observed secular variations in VM and PDO variabilities. For the sake of brevity, we show the results for the Hadley Center SST dataset. In the subsequent analysis, we concentrate on the low-frequency variability (>8 years) of the VM since it represents the primary factor driving the observed increase in VM variability.

In conjunction with the increased low-frequency variability of the VM, as anticipated, there has been a noticeable strengthening of the connections between the VM and various climate systems in the pan-North Pacific region and remote areas. These connections encompass concurrent winter–spring MHW intensity in the northeast Pacific, SAT in eastern North America, subsequent summer ITCZ precipitation, SSS in the Kuroshio–Oyashio Extension, western North Pacific TC frequency, and subsequent winter South China rainfall (see Data and Methods; Fig. 2). These findings suggest that the VM may have assumed a growing significance for climate systems across the Northern Hemisphere. A more comprehensive understanding of this heightened VM variability could provide valuable insights for climate prediction and projection.

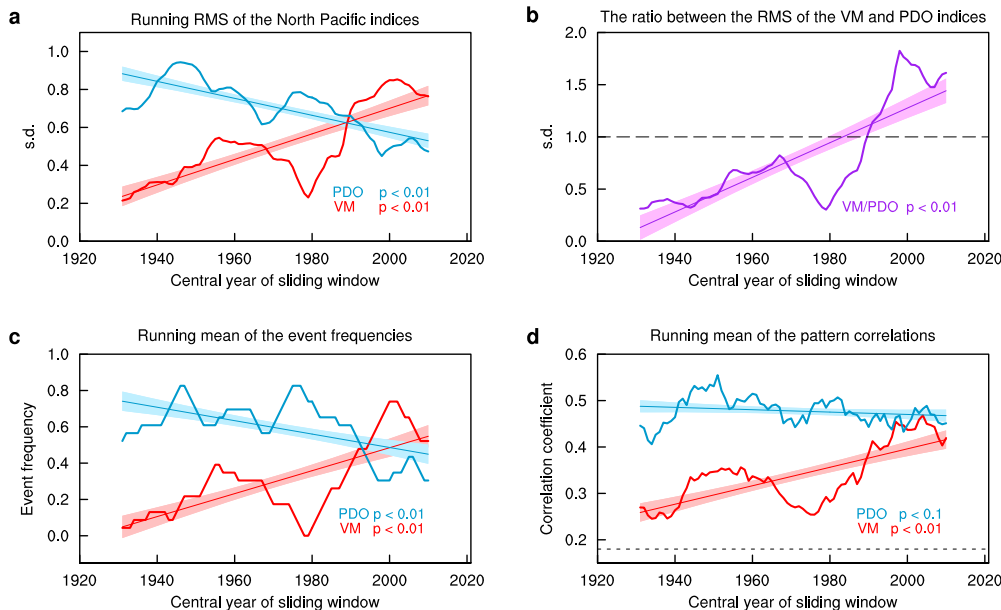


Fig. 1 | Increasing in the low-frequency VM variability in observations. **a** The 23-year running root-mean-square (RMS) of the boreal winter–spring (December–May, DJFMAM) low-frequency PDO (blue line) and VM (red line) indices for the period 1920–2021. **b** The secular variations in the ratio of the RMS of the VM and PDO indices. **c** The 23-year running mean of the PDO (blue line) and VM (red line) event frequencies. **d** The 23-year running mean pattern

correlation coefficients of the DJFMAM SST anomalies with PDO (blue line) and VM (red line) patterns in the North Pacific (20°N–70°N, 120°E–100°W). In **d** the horizontal dashed line indicates the 95% significance level for the running pattern correlations. Linear fits are displayed together with p values based on the Mann–Kendall test. The shaded areas in all panels indicate the two-sided 95% confidence levels of the slopes.

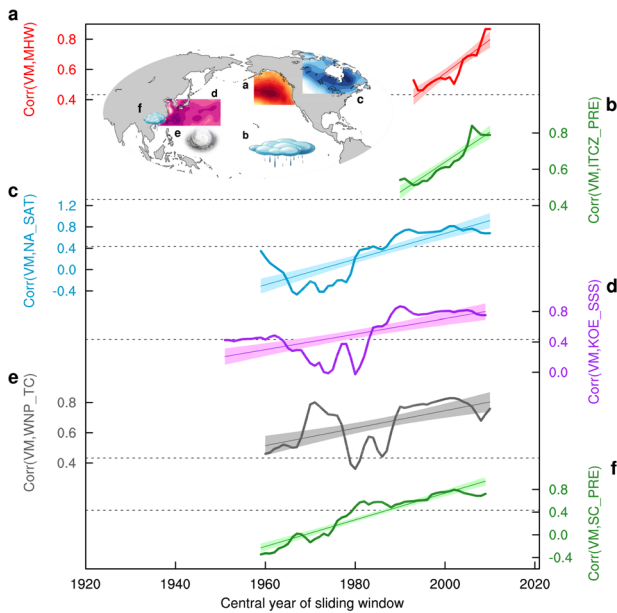


Fig. 2 | Enhanced connection between the VM and various climate indices. **a** The 23-year running correlation coefficients between the DJFMAM VM index and simultaneous northeast Pacific MHW intensity index for the period 1982–2021. **b** As in **a**, but for the JJA0 (where “0” refers to the current year) ITCZ precipitation index for the period 1979–2021. **c** As in **a**, but for the reverse simultaneous eastern North America (NA) SAT index for the period 1948–2021. **d** As in **a**, but for the JJA0 Kuroshio–Oyashio Extension (KOE) SSS index for the period 1940–2020. **e** As in **a**, but for the MJJAS0 western North Pacific (WNP) TC frequency index for the period 1949–2021. **f** As in **a**, but for the D0JFMAM1 (where “1” refers to the following year) South China (SC) rainfall index for the period 1948–2021. The horizontal dashed lines indicate the 95% significance level for the running correlations. Linear fits are displayed from the regression. All linear trends are significant at a 99% confidence level. The shaded areas indicate the two-sided 95% confidence levels of the slopes. Letters in the map on the upper left of the panel show the location of the various climate indices.

Mechanisms for the increased VM variability

The current question at hand revolves around identifying the underlying physical mechanisms responsible for the amplified low-frequency variability in VM. Previous studies have reported that tropical Pacific SST anomalies associated with CP El Niño can instigate low-frequency alterations in atmospheric patterns over the Hawaiian region, where the southern pole of the North Pacific Oscillation (NPO) is situated (see also Supplementary Fig. 7). These atmospheric changes, in turn, influence low-frequency fluctuations in the VM/NPGO by modulating surface heat fluxes^{33–35}. Significantly, there has been a noticeable escalation in the intensity and frequency of CP El Niño events since the 1980s to 1990s^{36–40}, closely coinciding with the period when low-frequency VM variability began to rise. The increased variability in CP SST during November–April is expected to have a growing impact on the sea level pressure (SLP) variability associated with the southern pole of the NPO, which is quantified by the Hawaii_SLP index during November–April (see Data and Methods; Fig. 3a). Consequently, the SLP variability connected to the southern pole of the NPO has also undergone a substantial strengthening (Fig. 3b). This, in turn, can play a role in driving the observed increase in low-frequency VM variability (see Data and Methods; Fig. 3c, d).

When we exclude the southern pole of the NPO by removing component of the VM forced by the NPO_S index using a simple one-dimensional (1D) auto-regressive (AR1) model (see Data and Methods), the residual low-frequency variability in VM no longer shows a significant upward trend (Supplementary Fig. 8). However, excluding the northern pole of the NPO still results in a significant increasing trend. Additionally, it’s worth noting that SST anomalies linked to the heightened low-frequency

VM variability display a particularly pronounced strengthening, primarily in the subtropical eastern North Pacific region (see Data and Methods; Supplementary Fig. 9), where SST anomalies are predominantly influenced by the southern pole of the NPO. These observations lead us to hypothesize that the increased VM variability may be attributed to the increased variability in CP SST.

This hypothesis has prompted us to investigate the potential impact of increased CP SST variability on VM variability using a 10-member pacemaker historical experiment with the Community Earth System Model Version 2 (CESM2), wherein SSTs in the tropical Pacific were adjusted to match observations (see Data and Methods). The results reveal robust correlations between the simulated Hawaii_SLP index and CP SST anomalies, indicating a strong influence of CP SST on atmospheric circulation in the Hawaiian region (see Supplementary Fig. 10). Furthermore, we observe significant positive correlations between the low-frequency (> 8 years) fluctuations in the ensemble mean simulated Hawaii_SLP index and those in the observed Hawaii_SLP index ($R = 0.71$, statistically significant at a 95% confidence level), along with a notable strengthening trend (Supplementary Fig. 11).

The simulated Hawaii_SLP index was then used to assess the impact of anomalous SST in the tropical Pacific on the heightened low-frequency VM variability as determined by the AR1 model (see Data and Methods). Notably, the low-frequency variability in the ensemble mean reconstructed VM index exhibits a significant correlation with that of the observed VM index ($R = 0.52$, statistically significant at the 95% confidence level; see Fig. 3e). Additionally, the low-frequency variability in the ensemble mean reconstructed VM index also demonstrates a noticeable increase (see Fig. 3f), although the upward trend is somewhat weaker in comparison to the observations (see Fig. 3d). In summary, these simulation results provide further evidence supporting the notion that increased CP SST variability is a key driver of the heightened VM variability observed in recent decades.

The increased CP SST variability has been primarily attributed to alterations in the mean state of the tropical Pacific associated with the increased stratification and shallowing thermocline in a warming climate^{37,41–45}. Furthermore, previous research has demonstrated that climate variability in the extratropical North Pacific, encompassing the VM/NPGO and the Pacific Meridional Mode, also promotes the emergence of CP ENSO^{17,21,22,46}. Di Lorenzo et al.⁴⁷ hypothesized the existence of a positive feedback loop between VM/NPGO and CP SST. According to this hypothesis, when CP SST variability increases in a response to changes in the tropical Pacific mean state, it could reinforce the positive feedback loop between VM/NPGO and CP SST, thereby contributing to heightened variability in both VM and CP SST. Further investigations are required to gain a more profound insight into the relative impacts of this positive feedback loop between the tropics and extratropics and changes in the tropical Pacific mean state on the increased VM variability.

Projections of future climate and VM change

The heightened VM variability observed over the last century raises a critical question: will VM variability continue to intensify in the context of future greenhouse warming? To explore this inquiry, we conducted an analysis of VM variability in a 30-member ensemble of the CESM Version 1 Large Ensemble (CESM1-LE) spanning from 1920 to 2100 under the RCP8.5 greenhouse scenario (details in Data and Methods). We compared the RMS of the VM index between two periods: the present (1920 to 2000) and the future (2020 to 2100). Remarkably, 24 out of 30 ensemble members (80%) projected increased VM variability in the future (Fig. 4a). The ensemble mean showed a notable increase of 10.1%, which surpassed the 95% confidence level according to a bootstrap test (Fig. 4a, d; see Data and Methods). Furthermore, we observed a concurrent projection of increased CP SST variability in the future climate (Fig. 4b, e), with strong consensus among 28 of the 30 ensemble members, aligning with recent studies⁴³. Notably, we discovered a correlation between the magnitude of CP SST variability increase and the strength of VM variability enhancement among CESM-LE members (correlation coefficient $R = 0.58$, significant at a 99% confidence

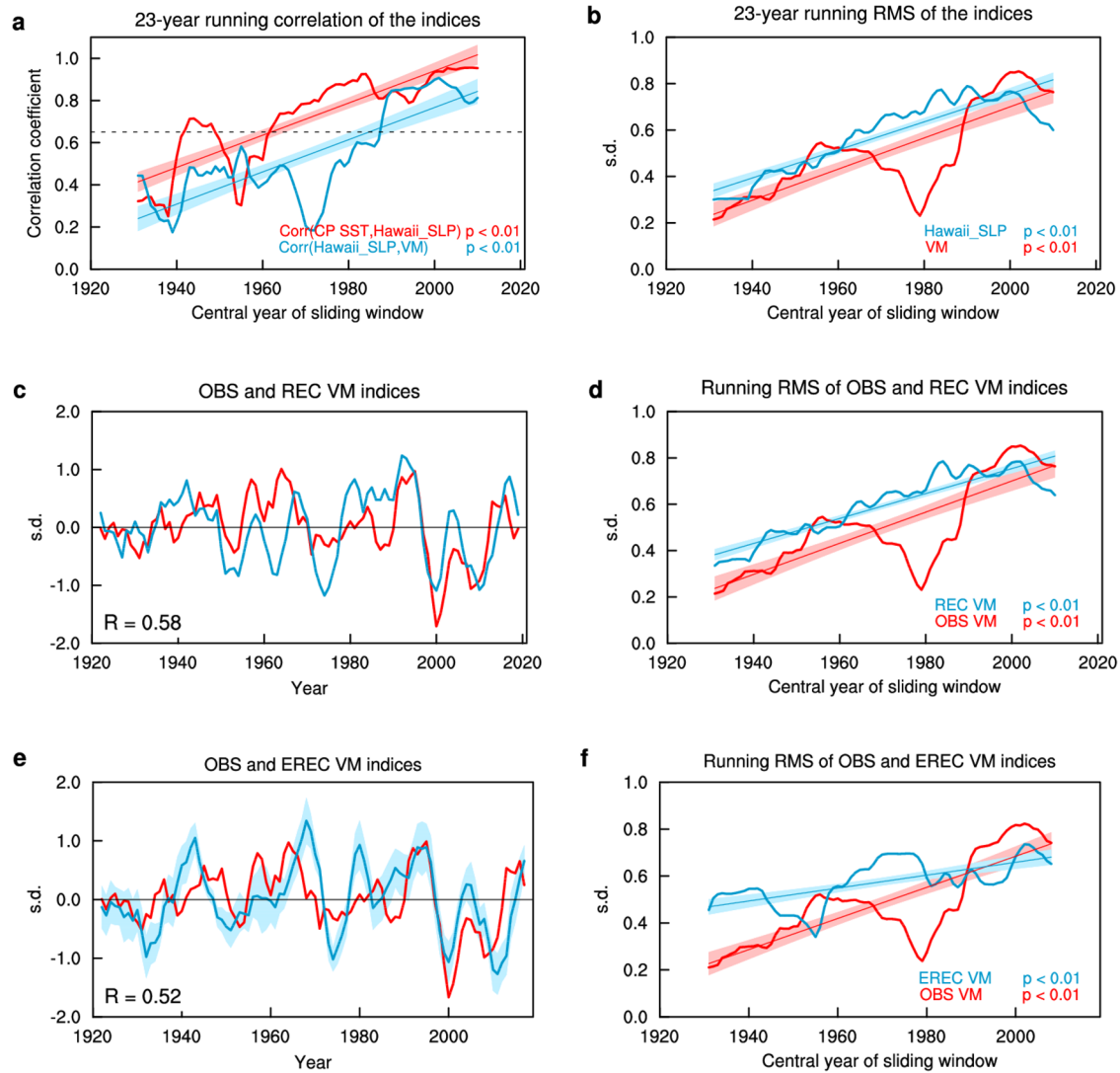


Fig. 3 | Mechanisms for the increased low-frequency VM variability. **a** The 23-year running correlation coefficients between the NDJFMA CP SST, NDJFMA Hawaii_SLP and DJFMAM VM indices for the period 1920–2021 in observations. **b** The 23-year running root-mean-square (RMS) of the NDJFMA Hawaii_SLP (blue line) and DJFMAM VM (red line) indices for the period 1920–2021. **c** The low-frequency fluctuations of DJFMAM observed (OBS) VM index (red line) and reconstructed (REC) VM index (blue line) using an AR1 model forced by the Hawaii_SLP index for the period 1920–2021. The units are in standard deviations (s.d.). **d** The 23-year running RMS of the DJFMAM OBS VM (red line) and REC VM

(blue line) indices. **e** The low-frequency of DJFMAM OBS VM index (red line) and the ensemble mean reconstructed (EREC) VM index (blue line) using an AR1 model forced by the simulated Hawaii_SLP index for the period 1920–2019. **f** The 23-year running RMS of the DJFMAM OBS VM (red line) and EREC VM (blue line) indices. In **a**, **b**, **d**, **f**, linear fits are displayed together with p values based on the Mann–Kendall test and the shaded areas indicate the two-sided 95% confidence levels of the slopes. In **c**, **e**, the correlation coefficients are given in the lower left corner of each panel, significant at a 95% confidence level. The shaded area in **e** represents the standard error.

level; Fig. 4c). This suggests that if greenhouse forcing amplifies CP SST variability, as witnessed in recent decades, a corresponding increase in VM variability can be expected.

Discussion

The VM variability, particularly over extended periods with low-frequency fluctuations, has displayed a notable upward trend in recent 4–5 decades. This heightened VM variability carries growing implications for climate systems across the pan-North Pacific and remote regions. Pacemaker model experiments demonstrate that the intensified variability in CP SST plays a pivotal role in amplifying the low-frequency variability of the VM through tropical-extratropical teleconnections. Consequently, if CP SST variability remains robustly on the rise under greenhouse warming^{37,42,43}, it is conceivable that VM variability will become more pronounced. The heightened VM variability holds promise for enhancing our ability to make future

climate predictions and projections, potentially mitigating the associated socioeconomic impacts of greenhouse warming.

It’s worth noting that, while both the low-frequency variabilities of the ensemble mean simulated Hawaii_SLP and the reconstructed VM indices from pacemaker experiments exhibit significant increases (see Fig. 3f and Supplementary Fig. 11b), these trends appear relatively weaker when compared to the observations (see Fig. 3d and Supplementary Fig. 11b). This highlights the pivotal role of CP SST in driving the augmented low-frequency VM variability, aligning with recent findings³⁵ that CP SST primarily contributes to VM variance on decadal and longer timescales. However, this doesn’t discount the potential contributions of other processes to the enhanced VM variability. Numerous extratropical factors, such as changing Arctic sea ice^{48,49} and the Kuroshio–Oyashio Extension^{50,51}, could also be influencing the increased VM variability. Investigating the relative significance of these factors in driving VM fluctuations is essential

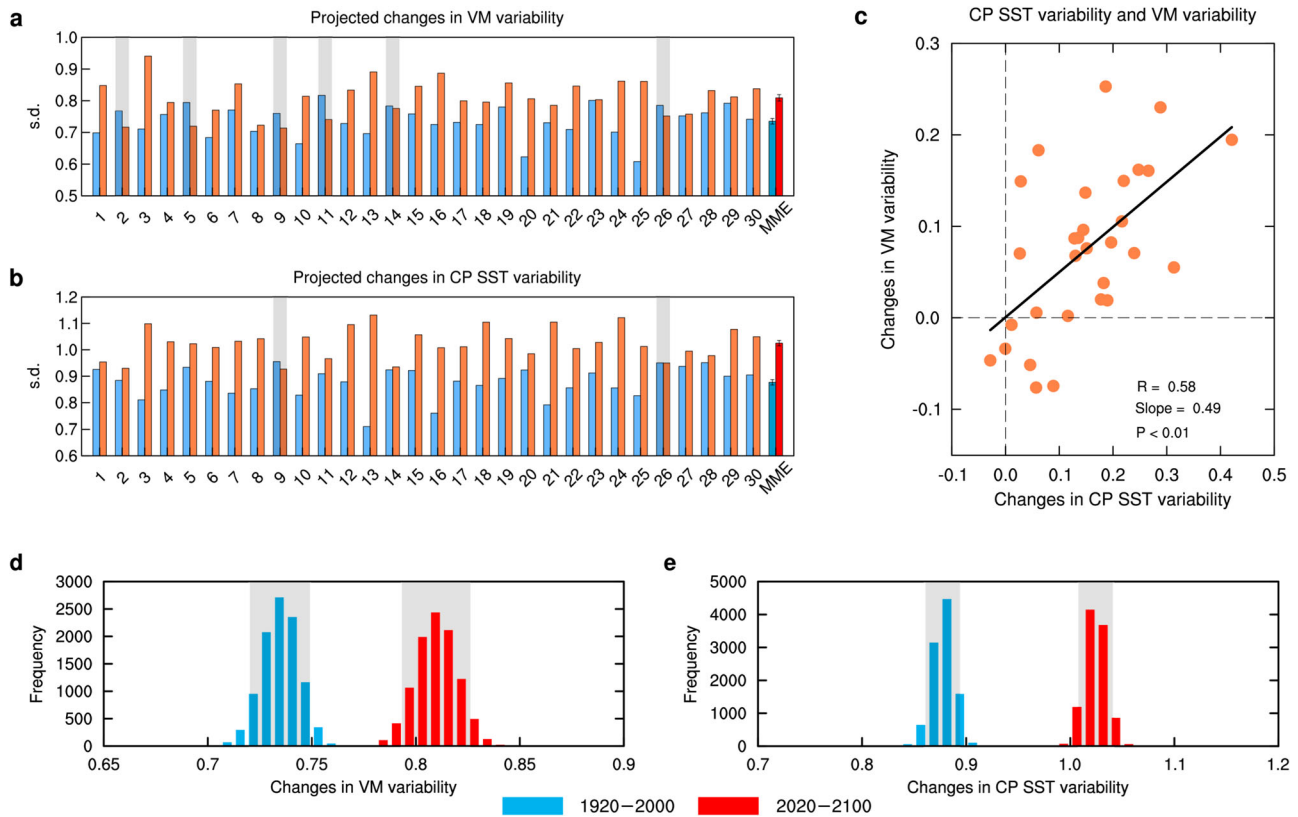


Fig. 4 | Projected changes in VM and CP SST variability. Comparison of the low-frequency VM (a) and CP SST (b) variabilities over the present (1920 to 2000, blue bars) and future (2020 to 2100, red bars) periods in the 30 members of the CESM-LE. The multimember ensemble means over the present and future periods are also shown. Error bars are calculated as 1.0 s.d. of a total of 10,000 inter-realizations of a bootstrap method (see Data and Methods). Members that simulate a decrease are

grayed out. Variabilities of the VM and CP SST are projected to increase under greenhouse warming. c Intermember relationships between changes in VM variability and CP SST variability. A linear fit is shown together with the correlation coefficient R, slope, and P values from the regression. Histograms of 10,000 realizations of a bootstrap method for the VM (d) and CP SST (e) variabilities. The gray shaded areas refer to the respective 1.0 s.d. of the 10,000 realizations.

for achieving a comprehensive understanding of the complex interplay among these processes and their impacts on VM variability.

This study primarily focuses on the heightened VM variability over a century-long timeframe, leaving the underlying mechanisms responsible for the diminished variability of the PDO unaddressed. Recent studies^{52,53} research has proposed that in a warming climate, the decadal variability of the PDO is considerably suppressed due to the acceleration of oceanic Rossby waves, potentially linked to enhanced oceanic stratification caused by greenhouse forcing. Given the substantial influence of the PDO on global climate patterns, further investigations are warranted to gain a better grasp of the factors contributing to the reduced PDO variability in the context of a changing climate.

Methods

Observed Data

We used four monthly SST datasets^{54–57} in this study: (1) the Hadley Center Sea Ice and SST dataset version 1.1 (HadISST v1.1; 1871–2021)⁵⁴; (2) the National Oceanic and Atmospheric Administration Extended Reconstructed SST version 5 (ERSST v5; 1854–2021)⁵⁵; (3) the Centennial in situ Observation-Based Estimates SST version 2 (COBE SST; 1850–2021)⁵⁶; and (4) the Kaplan Extended SST version 2 (Kaplan SST v2; 1856–2021)⁵⁷. The SLP fields were derived from two “merged” atmospheric reanalysis datasets. The merged NCEP dataset was made from the NOAA-CIRES-DOE Twentieth Century Reanalysis (20CRv3; 1836–2015)⁵⁸ and NCEP/DOE Reanalysis 2 (1979–2021)⁵⁹. To ensure temporal consistency, the differences in monthly climatology between 20CRv3 and NCEP/DOE2 data during the overlap period 1979–2015 were used to calibrate the mean state of NCEP/DOE2. The monthly mean SAT data were from NCEP–NCAR Reanalysis 1

(1948–2021)⁶⁰. The global precipitation data were from the Global Precipitation Climatology Project (GPCP; 1979–2021)⁶¹. The Precipitation Reconstruction over Land (PREC/L) dataset was developed by the Climate Prediction Center (CPC) on a 1° grid (1948–2021)⁶². TC best-track data were produced by the CMA/China Meteorological Data Service Center (https://tcdata.typhoon.org.cn/zjljsjj_zlhq.html)^{63,64}. A daily dataset of global MHW from 1982 to 2021 was available from the Science Data Bank (<https://www.scidb.cn/en/s/nqauYn#p4>)⁶⁵. The Institute of Atmospheric Physics (IAP) ocean gridded products provide global salinity data at a resolution of 1° × 1° and 41 vertical levels from 1 m to 2000 m (1940–2020) (<http://159.226.119.60/cheng>)⁶⁶.

Climate indices

To examine variation in the VM and PDO indices, we performed Empirical Orthogonal Function (EOF) analysis of the monthly SST anomalies in the extratropical North Pacific (20°N–65°N, 124°E–100°W) for the period 1920–2021 (after removing the monthly mean global average SST anomalies). The PDO and VM indices are defined as the principal component (PC) time series of the first and second leading EOF, respectively¹⁵. Then, we extracted the low-frequency (>8 years) components of these indices by using 8-year low-pass filter based on the fast Fourier transform filter for these indices. The NPGO index is defined as the PC time series of the second leading EOF of SSH anomalies over the northeast Pacific (25°N–62°N, 180°–110°W), which is available at <http://www.o3d.org/npgo> for the period 1950–2021¹⁶. The CP SST index is used to represent CP ENSO. We applied an EOF analysis to the quadratically detrended SST anomalies of the tropical Pacific (15°S–15°N, 140°E–80°W). The leading two PCs (PC1 and PC2) of the EOF analysis correspond to a respective positive phase of EOF1 (a warm

anomaly center in the central eastern Pacific) and EOF2 (a warm anomaly center in the central Pacific and a cool anomaly aside). The CP SST index is then defined by $(PC1 + PC2)/\sqrt{2}$ ⁶⁷. The Hawaii_SLP index is calculated as the average of SLP anomalies over the Hawaiian region (16°N–24°N, 157°W–130°W; see also Supplementary Fig. 6). The southern pole of the NPO (NPO_S) index is the same as the Hawaii_SLP index. The northern pole of the NPO (NPO_N) index is defined as SLP anomalies averaged over the northern pole of the NPO (48°N–63°N, 165°W–135°W; see also Supplementary Fig. 6).

We also defined various climate indices as domain-averaged variables in the prescribed regions, including the northeast Pacific MHW intensity index, eastern North America SAT index, ITCZ precipitation index, Kuroshio–Oyashio Extension SSS index, western North Pacific TC frequency index and South China rainfall index. The detailed definitions of these climate indices are provided in Supplementary Table 1. All indices have been quadratically detrended and filtered by performing 8-year low-pass filter before analysis.

Root-mean-square (RMS)

To explore the variability of the PDO, VM, and NPGO indices, we applied the RMS analysis for these indices:

$$RMS = \sqrt{\frac{\sum_{i=1}^N X_i^2}{N}}, \quad (1)$$

where X represents the variables (such as the VM index), and N denotes the number of available time series of the variables⁶⁸.

SST variance

To further elucidate the changes in the spatial structure of the SST anomalies associated with the increased VM variability, we extracted the North Pacific SST anomaly variances explained by the VM by calculating the correlation square of the North Pacific SST anomalies with the VM index for the periods 1950–1980 and 1990–2020, respectively.

Autoregressive model

The oceanic VM response to atmospheric forcing is quantified using an autoregressive model of order 1 (AR1)^{17,69,70}:

$$VM_{t+1} = \alpha \cdot Hawaii_SLP_t + \beta \cdot VM_t + \eta_t, \quad (2)$$

where the first and second terms on the right-hand side represent the SLP forcing over the Hawaiian region and the damping term, respectively, and η_t is uncorrelated noise. The coefficients α and β are obtained by regressing the VM against the previous month's Hawaii_SLP, removing the Hawaii_SLP term, and then regressing the residual against the previous month's VM.

CESM2 tropical pacific pacemakers

We analyzed a 10-member ensemble of CESM2 (1-degree spatial resolution) simulations in which time-evolving SST anomalies in the central-eastern tropical Pacific are nudged to observations (ERSST v5) during 1880–2019. In each pacemaker run, the observed evolution of the tropical Pacific is maintained (i.e., the tropical Pacific is the pacemaker), with the rest of the model's coupled climate system free to evolve. The nudging mask for the CESM2 pacemakers covered the tropical Pacific from the American coast to the western Pacific, with the form of a wedge shape toward the Maritime Continent to the west of the dateline. The nudging is full strength between 15° S–15° N with a 5-degree latitude buffer region to the south and north where the strength of the relaxation is linearly reduced (see https://www.cesm.ucar.edu/working_groups/CVC/simulations/cesm2-pacific_pacemaker.html for the nudging mask area and the details of the Pacific Pacemaker experiments)⁷¹.

CESM1 large ensemble data archive

We used the outputs of 30 members of the CESM1-LE simulations from 1920–2100 under the RCP8.5 greenhouse scenario. The 30-member ensemble uses historical radiative forcing for the period 1920–2005 and RCP8.5 radiative forcing thereafter. These data are available at <https://www2.cesm.ucar.edu/models/experiments/LENS2>.

Significance tests

The statistical significance of the correlations and regressions was determined using a two-tailed Student's t -test. The significance of linear trends is determined using the Mann–Kendall test, which is a non-parametric test used to detect the presence of linear or non-linear trends in time series. The shaded areas in Figs. 1, 3a, b, d, f and Supplementary Figs. 2, 4a, 5, 8 and 11b are the two-sided 95% confidence bounds. The shaded areas in Fig. 3e and Supplementary Figs. 10c and 11a represent the standard error. Bootstrap test⁷² was conducted to examine whether the changes in the VM and CP SST variabilities are statistically significant under greenhouse warming. A total of 10,000 realizations are conducted to obtain the mean from the 30 members. Each realization is averaged over 30 samples that are independently and randomly resampled from the 30 members. In this resampling process, any model is allowed to be selected more than once. The standard deviation (s.d.) of the 10,000 realizations is calculated for each period. If the mean value difference between the future and present periods is greater than the sum of the two separate 10,000-realization s.d. values, then the change is statistically significant above 95% confidence level.

Data availability

The data that support the findings of this study are freely available. The HadISST dataset is available at <https://www.metoffice.gov.uk/hadobs/hadisst/>. The ERSST dataset is available at <https://psl.noaa.gov/data/gridded/data.noaa.ersst.v5.html>. The Kaplan SST dataset is available at https://psl.noaa.gov/data/gridded/data.kaplan_sst.html. The COBE SST dataset is available at <https://psl.noaa.gov/data/gridded/data.cobe2.html>. The 20CRv3 dataset is available at https://psl.noaa.gov/data/gridded/data.20thC_ReanV3.html. The NCEP-DOE Reanalysis 2 is available at <https://psl.noaa.gov/data/gridded/data.ncep.reanalysis2.html>. The NCEP/NCAR Reanalysis 1 is available at <https://psl.noaa.gov/data/gridded/data.ncep.reanalysis.html>. The GPCP dataset is available at <https://psl.noaa.gov/data/gridded/data.gpcp.html>. The PREC/L dataset is available at <https://psl.noaa.gov/data/gridded/data.prec.l.html>. TC best-track dataset is available at https://tcdata.typhoon.org.cn/zjljsjj_zlhq.html. The global MHW dataset is available at <https://www.scidb.cn/en/s/nqauYn#p4>. The global salinity dataset is available at <http://159.226.119.60/cheng>.

Code availability

The data in this study were analyzed with NCAR Command Language (NCL; <http://www.ncl.ucar.edu/>). All relevant codes used in this study are available, upon request, from the corresponding author R.Q.D.

Received: 1 December 2023; Accepted: 15 February 2024;

Published online: 27 February 2024

References

- Messié, M. & Chavez, F. Global modes of sea surface temperature variability in relation to regional climate indices. *J. Clim.* **24**, 4314–4331 (2011).
- Di Lorenzo, E. & Mantua, N. Multi-year persistence of the 2014/15 North Pacific marine heatwave. *Nat. Clim. Change* **6**, 1042–1047 (2016).
- Trenberth, K. E., Fasullo, J. T., Branstator, G. & Phillips, A. S. Seasonal aspects of the recent pause in surface warming. *Nat. Clim. Change* **4**, 911–916 (2014).
- Mantua, N. J. et al. A Pacific interdecadal climate oscillation with impacts on salmon production. *Bull. Am. Meteorol. Soc.* **78**, 1069–1080 (1997).

5. Zhang, Y., Wallace, J. M. & Battisti, D. S. ENSO-like interdecadal variability: 1900–93. *J. Clim.* **10**, 1004–1020 (1997).
6. Newman, M. et al. The Pacific Decadal Oscillation, revisited. *J. Clim.* **29**, 4399–4427 (2016).
7. Deser, C., Phillips, A. C. & Hurrell, J. W. Pacific interdecadal climate variability: linkages between the tropics and the North Pacific during boreal winter since 1900. *J. Clim.* **17**, 3109–3124 (2004).
8. Yeh, S.-W., Kang, Y.-J., Noh, Y. & Miller, A. J. The North Pacific climate transitions of the winters of 1976/77 and 1988/89. *J. Clim.* **24**, 1170–1183 (2011).
9. Miller, A. J. & Schneider, N. Interdecadal climate regime dynamics in the North Pacific ocean: theories, observations and ecosystem impacts. *Prog. Oceanogr.* **47**, 355–379 (2000).
10. Kosaka, Y. & Xie, S. P. Recent global-warming hiatus tied to equatorial Pacific surface cooling. *Nature* **501**, 403 (2013).
11. Dai, A. Increasing drought under global warming in observations and models. *Nat. Clim. Change* **3**, 52–58 (2013).
12. Kosaka, Y. & Xie, S. P. The tropical Pacific as a key pacemaker of the variable rates of global warming. *Nat. Geosci.* **9**, 669–673 (2016).
13. Deser, C. et al. Uncertainty in climate change projections: the role of internal variability. *Clim. Dynam.* **38**, 527–546 (2012).
14. Wu, Z. & Lin, H. Interdecadal Variability of the ENSO-North Atlantic Oscillation Connection in boreal summer. *Quart. J. Roy. Meteor. Soc.* **138**, 1668–1675 (2012).
15. Bond, N. A., Overland, J. E., Spillane, M. & Stabeno, P. Recent shifts in the state of the North Pacific. *Geophys. Res. Lett.* **30**, 2183 (2003).
16. Di Lorenzo, E. et al. North Pacific Gyre Oscillation links ocean climate and ecosystem change. *Geophys. Res. Lett.* **35**, L08607 (2008).
17. Ding, R., Li, J., Tseng, Y., Sun, C. & Guo, Y. The Victoria mode in the North Pacific linking extratropical sea level pressure variations to ENSO. *J. Geophys. Res.* **120**, 27–45 (2015).
18. Vimont, D. J., Wallace, J. M. & Battisti, D. S. The seasonal footprinting mechanism in the Pacific: implications for ENSO. *J. Clim.* **16**, 2668–2675 (2003).
19. Anderson, B. T. Tropical Pacific sea-surface temperatures and preceding sea level pressure anomalies in the subtropical North. *Pac. J. Geophys. Res.* **108**, 4732 (2003).
20. Ji, K., Tseng, Y., Ding, R., Mao, J. & Feng, L. Relative contributions to ENSO of the seasonal footprinting and trade wind charging mechanisms associated with the Victoria mode. *Clim. Dynam.* **60**, 47–63 (2023).
21. Yu, J. Y., Kao, H. Y. & Lee, T. Subtropics-related interannual sea surface temperature variability in the central equatorial Pacific. *J. Clim.* **23**, 2869–2884 (2010).
22. Yu, J. Y. & Kim, S. T. Relationships between extratropical sea level pressure variations and the Central Pacific and Eastern Pacific types of ENSO. *J. Clim.* **24**, 708–720 (2011).
23. Ding, R., Li, J., Tseng, Y. & Ruan, C. Influence of the North Pacific Victoria mode on the Pacific ITCZ summer precipitation. *J. Geophys. Res.* **120**, 964–979 (2015).
24. Lin, R., Li, Y. & Ding, R. Relationship between Victoria Mode and Northeast Pacific Marine Heatwave. *J. Chengdu Univ. Inf. Technol.* **38**, 200–207 (2023). (Chinese).
25. Zhao, Y. & Yu, J. Two Marine Heat Wave (MHW) Variants under a Basin-wide MHW Conditioning Mode in the North Pacific and Their Atlantic Associations. *J. Clim.* **36**, 8657–8674 (2023).
26. Pu, X., Chen, Q., Zhong, Q., Ding, R. & Liu, T. Influence of the North Pacific Victoria mode on western North Pacific tropical cyclone genesis. *Clim. Dynam.* **52**, 245–256 (2019).
27. Li, J. et al. Winter particulate pollution severity in North China driven by atmospheric teleconnections. *Nat. Geosci.* **15**, 349–355 (2022).
28. Zou, Q. et al. Is the North Pacific Victoria mode a predictor of winter rainfall over South China? *J. Clim.* **33**, 8833–8847 (2020).
29. Ji, K. & Ding, R. Interannual impact of the Victoria mode on the winter-spring surface air temperature over Eurasia and North America. *npj Clim. Atmos. Sci.* **6**, 114 (2023).
30. Ge, Y. & Luo, D. Winter cold extremes over the eastern North America: Pacific origins of interannual-to-decadal variability. *Environ. Res. Lett.* **18**, 054006 (2023).
31. Di Lorenzo, E. et al. Nutrient and salinity decadal variations in the central and eastern North Pacific. *Geophys. Res. Lett.* **36**, L14601 (2009).
32. Di Lorenzo, E. et al. Modes and mechanisms of Pacific decadal-scale variability. *Ann. Rev. Mar. Sci.* **15**, 249–275 (2022).
33. Di Lorenzo, E. et al. Central Pacific El Niño and decadal climate change in the North Pacific Ocean. *Nat. Geosci.* **3**, 762–765 (2010).
34. Furtado, J. C., Di Lorenzo, E., Anderson, B. T. & Schneider, N. Linkages between the North Pacific Oscillation and central tropical Pacific SSTs at low frequencies. *Clim. Dynam.* **39**, 2833–2846 (2012).
35. Li, Z., Ding, R., Mao, J. & Ren, Z. Understanding the Driving Forces of the North Pacific Victoria Mode. *J. Clim.* **36**, 6547–6560 (2023).
36. Lee, T. & McPhaden, M. J. Increasing intensity of El Niño in the central-equatorial Pacific. *Geophys. Res. Lett.* **37**, L14603 (2010).
37. Yeh, S.-W. et al. El Niño in a changing climate. *Nature* **461**, 511–514 (2009).
38. Yu, J.-Y. et al. Linking emergence of the Central-Pacific El Niño to the Atlantic Multi-decadal Oscillation. *J. Clim.* **28**, 651–662 (2015).
39. Freund, M. B. et al. Higher frequency of Central Pacific El Niño events in recent decades relative to past centuries. *Nat. Geosci.* **12**, 450–455 (2019).
40. Capotondi, A. et al. Understanding ENSO diversity. *Bull. Am. Meteorol. Soc.* **96**, 921–938 (2015).
41. Kim, S. T. & Yu, J.-Y. The two types of ENSO in CMIP5 models. *Geophys. Res. Lett.* **39**, L11704 (2012).
42. Cai, W. et al. Increased variability of eastern Pacific El Niño under greenhouse warming. *Nature* **564**, 201–206 (2018).
43. Cai, W. et al. Increased ENSO sea surface temperature variability under four IPCC emission scenarios. *Nat. Clim. Change* **12**, 228–231 (2022).
44. Hu, Z.-Z. et al. The interdecadal shift of ENSO properties in 1999/2000: a review. *J. Clim.* **33**, 4441–4462 (2020).
45. Li, Y. et al. Impacts of the Tropical Pacific Cold Tongue Mode on ENSO Diversity Under Global Warming. *J. Geophys. Res.* **122**, 8524–8542 (2017).
46. Chang, P. et al. Pacific meridional mode and El Niño–Southern Oscillation. *Geophys. Res. Lett.* **34**, L16608 (2007).
47. Di Lorenzo, E. et al. ENSO and meridional modes: a null hypothesis for Pacific climate variability. *Geophys. Res. Lett.* **42**, 9440–9448 (2015).
48. Bonan, D. B., Lehner, F. & Holland, M. M. Partitioning uncertainty in projections of Arctic sea ice. *Environ. Res. Lett.* **16**, 044002 (2021).
49. Kennel, C. F. & Yulaeva, E. Influence of Arctic sea-ice variability on Pacific trade winds. *Proc. Natl Acad. Sci.* **117**, 2824–2834 (2020).
50. Joh, Y. & Di Lorenzo, E. Interactions between Kuroshio Extension and Central Tropical Pacific lead to preferred decadal-timescale oscillations in Pacific climate. *Sci. Rep.* **9**, 13558 (2019).
51. Joh, Y., Di Lorenzo, E., Siqueira, L. & Kirtman, B. P. Enhanced interactions of Kuroshio Extension with tropical Pacific in a changing climate. *Sci. Rep.* **11**, 6247 (2021).
52. Fang, C., Wu, L. & Zhang, X. The impact of global warming on the Pacific Decadal Oscillation and the possible mechanism. *Adv. Atmos. Sci.* **31**, 118–130 (2014).
53. Geng, T., Yang, Y. & Wu, L. On the mechanisms of Pacific decadal oscillation modulation in a warming climate. *J. Clim.* **32**, 1443–1459 (2019).
54. Rayner, N. A. et al. Global analyses of sea surface temperature, sea ice, and night marine air temperature since the late nineteenth century. *J. Geophys. Res.* **108**, 4407 (2003).

55. Huang, B. et al. Extended Reconstructed Sea Surface Temperature version 5 (ERSSTv5), upgrades, validations, and intercomparisons. *J. Clim.* **30**, 8179–8205 (2017).
56. Hirahara, S., Ishii, M. & Fukuda, Y. Centennial-scale sea surface temperature analysis and its uncertainty. *J. Clim.* **27**, 57–75 (2014).
57. Kaplan, A. et al. Analyses of global sea surface temperature 1856–1991. *J. Geophys. Res.* **103**, 18567–18589 (1998).
58. Slivinski, L. C. et al. Towards a more reliable historical reanalysis: Improvements for version 3 of the Twentieth Century Reanalysis. *Syst. Q. J. Roy. Meteorol. Soc.* **145**, 2876–2908 (2019).
59. Kanamitsu, M. et al. NCEP-DOE AMIP-II Reanalysis (R-2). *Bull. Am. Meteor. Soc.* **83**, 1631–1643 (2002).
60. Kalnay, E. et al. The NCEP/NCAR 40-year reanalysis project. *Bull. Am. Meteorol. Soc.* **77**, 437–470 (1996).
61. Adler, R. F. et al. The version 2 Global Precipitation Climatology Project (GPCP) monthly precipitation analysis (1979–present). *J. Hydrometeor.* **4**, 1147–1167 (2003).
62. Chen, M. Y., Xie, P. P., Janowiak, J. E. & Arkin, P. A. Global land precipitation: a 50-yr monthly analysis based on gauge observations. *J. Hydrometeor.* **3**, 249–266 (2002).
63. Ying, M. et al. An overview of the China Meteorological Administration tropical cyclone database. *J. Atmos. Ocean. Technol.* **31**, 287–301 (2014).
64. Lu, X. et al. Western North Pacific tropical cyclone database created by the China Meteorological Administration. *Adv. Atmos. Sci.* **38**, 690–699 (2021).
65. Zhang, X. et al. Observed Frequent Occurrences of Marine Heatwaves in Most Ocean Regions during the Last Two Decades. *Adv. Atmos. Sci.* **39**, 1579–1587 (2022).
66. Cheng, L. et al. Improved estimates of changes in upper ocean salinity and the hydrological cycle. *J. Clim.* **33**, 10357–10381 (2020).
67. Takahashi, K., Montecinos, A., Goubanova, K. & Dewitte, B. ENSO regimes: reinterpreting the canonical and Modoki El Niño. *Geophys. Res. Lett.* **38**, L10704 (2011).
68. Yeh, S.-W., Wang, X., Wang, C. & Dewitte, B. On the relationship between the North Pacific climate variability and the Central Pacific El Niño. *J. Clim.* **28**, 663–677 (2015).
69. Newman, M., Compo, G. P. & Alexander, M. A. ENSO-forced variability of the Pacific Decadal Oscillation. *J. Clim.* **16**, 3853–3857 (2003).
70. Schneider, N. & Cornuelle, B. D. The forcing of the Pacific Decadal Oscillation. *J. Clim.* **18**, 4355–4373 (2005).
71. Danabasoglu, G. et al. The Community Earth System Model Version 2 (CESM2). *J. Adv. Model. Earth Syst.* **12**, e2019MS001916 (2020).
72. Kay, J. E. et al. The Community Earth System Model (CESM) large ensemble project: a community resource for studying climate change in the presence of internal climate variability. *Bull. Am. Meteorol. Soc.* **96**, 1333–1349 (2015).
73. Austin, P. C. & Tu, J. V. Bootstrap methods for developing predictive models. *Am. Stat.* **58**, 131–137 (2004).

Acknowledgements

This research was jointly supported by the National Natural Science Foundation of China (42225501, 41975070), and China's National Key Research and Development Projects (2020YFA0608402). The authors thank Prof. Zhongshi Zhang for his constructive comments that helped to improve the paper.

Author contributions

K.J. and R.Q.D. designed and wrote the paper. K.J. performed the data analysis and prepared all figures. J.-Y.Y., J.P.L., Z.-Z.H., Y.-H.T., J.S., Y.Y.Z., and C.S. contributed to the interpretation of the results and the improvement of the manuscript.

Competing interests

The authors declare no competing interests.

Additional information

Supplementary information The online version contains supplementary material available at <https://doi.org/10.1038/s41612-024-00599-0>.

Correspondence and requests for materials should be addressed to Ruiqiang Ding.

Reprints and permissions information is available at <http://www.nature.com/reprints>

Publisher's note Springer Nature remains neutral with regard to jurisdictional claims in published maps and institutional affiliations.

Open Access This article is licensed under a Creative Commons Attribution 4.0 International License, which permits use, sharing, adaptation, distribution and reproduction in any medium or format, as long as you give appropriate credit to the original author(s) and the source, provide a link to the Creative Commons licence, and indicate if changes were made. The images or other third party material in this article are included in the article's Creative Commons licence, unless indicated otherwise in a credit line to the material. If material is not included in the article's Creative Commons licence and your intended use is not permitted by statutory regulation or exceeds the permitted use, you will need to obtain permission directly from the copyright holder. To view a copy of this licence, visit <http://creativecommons.org/licenses/by/4.0/>.

© The Author(s) 2024